Achieving Self-supported Nanoporous Cu Catalysts with Good Conductivity for Hydrogen Evolution via Dealloying Amorphous Ribbons

Ziwei Guo[ab], Jiameng Sun[b], Qi Chen[ab], Zhigang Qi[ab], Zhaoxuan Wang[ab], Xinlong Lu[ab], Yanxu Li[ab], Zhicheng Yan[c], Guanhua Cheng[b], Weimin Wang*[ab]

a. State Key Laboratory of Coatings for Advanced Equipment, School of Materials Science and Engineering, Shandong University, Jinan, 250061, China.
b. Key Laboratory for Liquid-Solid Structural Evolution and Processing of Materials (Ministry of Education), Shandong University, Jinan, 250061, China.
c. State Grid Shandong Electric Power Research Institute, Jinan, 250002, China.

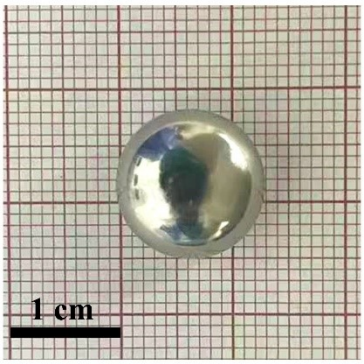

Figure S1 The photograph of $Cu_{57}Au_3Ti_{40}$ alloy ingot.

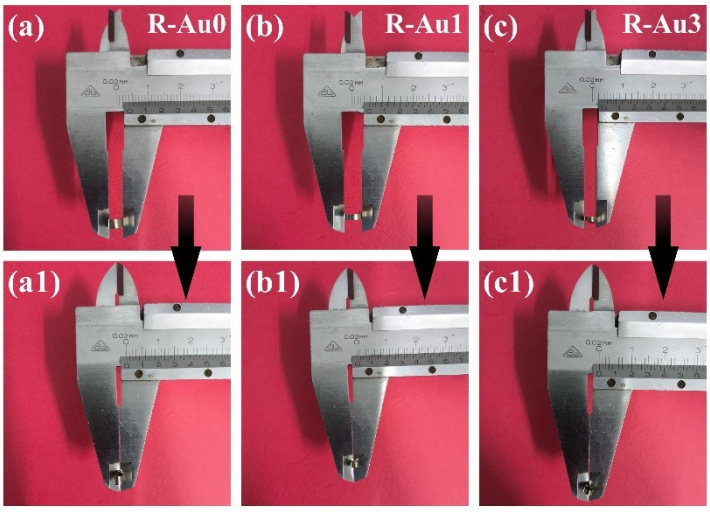

Figure S2 The photograph of R-Au0 ribbon (a, a1), R-Au1 ribbon (b, b1), R-Au3 ribbon (c, c1).

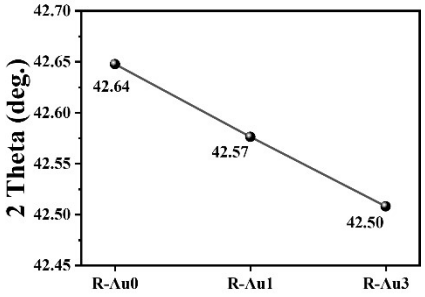

Figure S3 Diffuse scattering peak position of the as-spun ribbons.

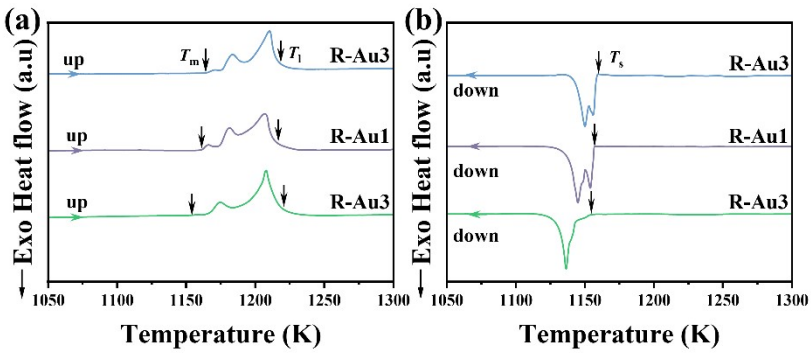

Figure S4 DSC curves of as-spun ribbons in the high-temperature region: (a) heating stage, (b) cooling stage.

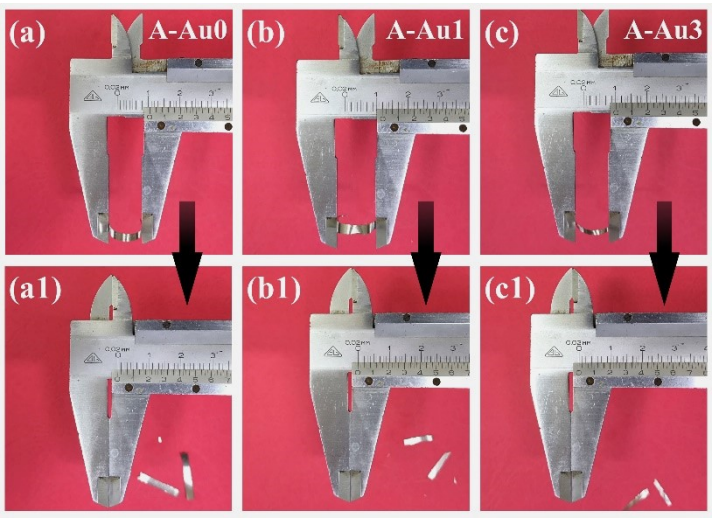

Figure S5 The photograph of A-Au0 ribbon (a, a1), A-Au1 ribbon (b, b1), A-Au3 ribbon (c, c1).

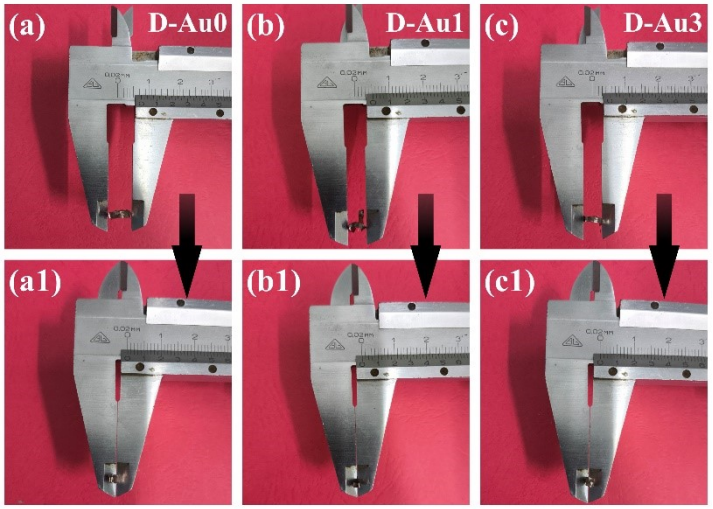

Figure S6 The photograph of D-Au0 ribbon (a, a1), D-Au1 ribbon (b, b1), D-Au3 ribbon (c, c1).

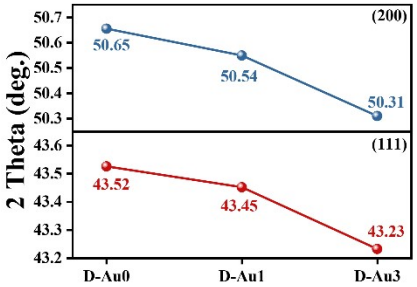

Figure S7 Diffuse scattering peak position of the as-dealloyed ribbons.

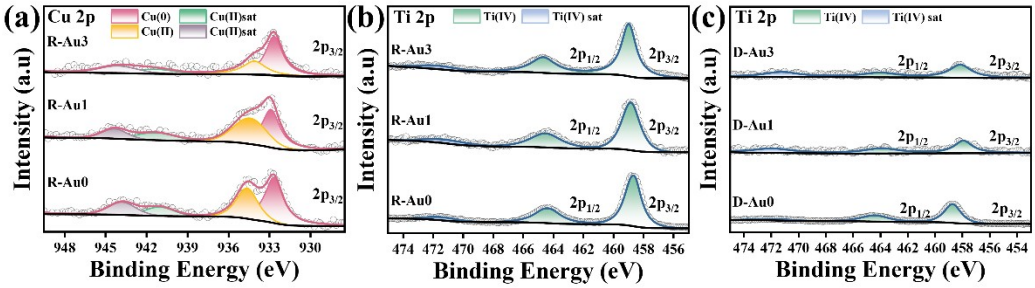

Figure S8 (a) Cu 2p and (b)Ti 2p spectra of the as-spun ribbons, (c) Ti 2p spectra of the as-dealloyed ribbons.

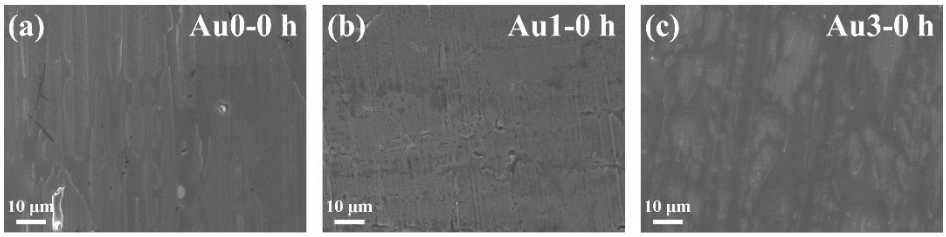

Figure S9 Plan-view SEM images of R-Au0 (a), R-Au1 (b), R-Au3 (c) before dealloying.

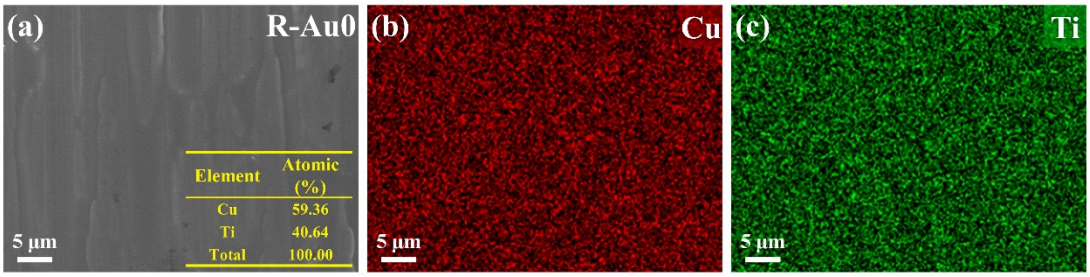

Figure S10 (a) Plain-view SEM image and EDX result of the plane, (b,c) corresponding elemental mapping images of R-Au0.

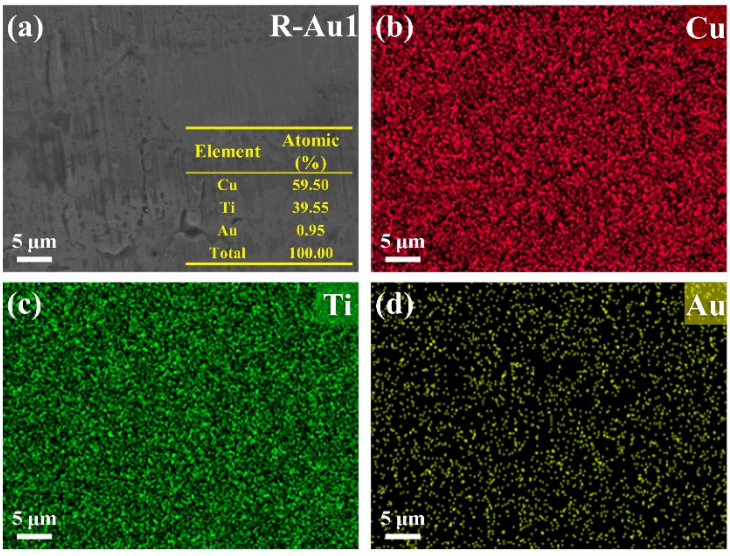

Figure S11 (a) Plain-view SEM image and EDX result of the plane, (b-d) corresponding elemental

mapping images of R-Au1.

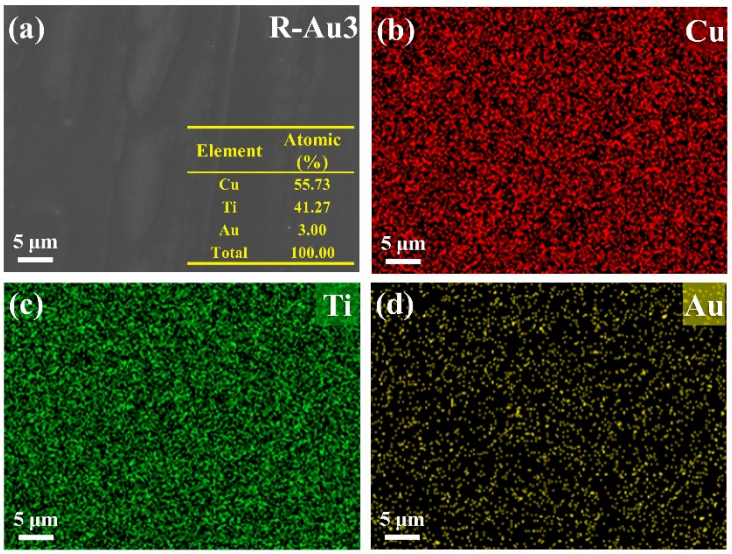

Figure S12 (a) Plain-view SEM image and EDX result of the plane, (b-d) corresponding elemental mapping images of R-Au3.

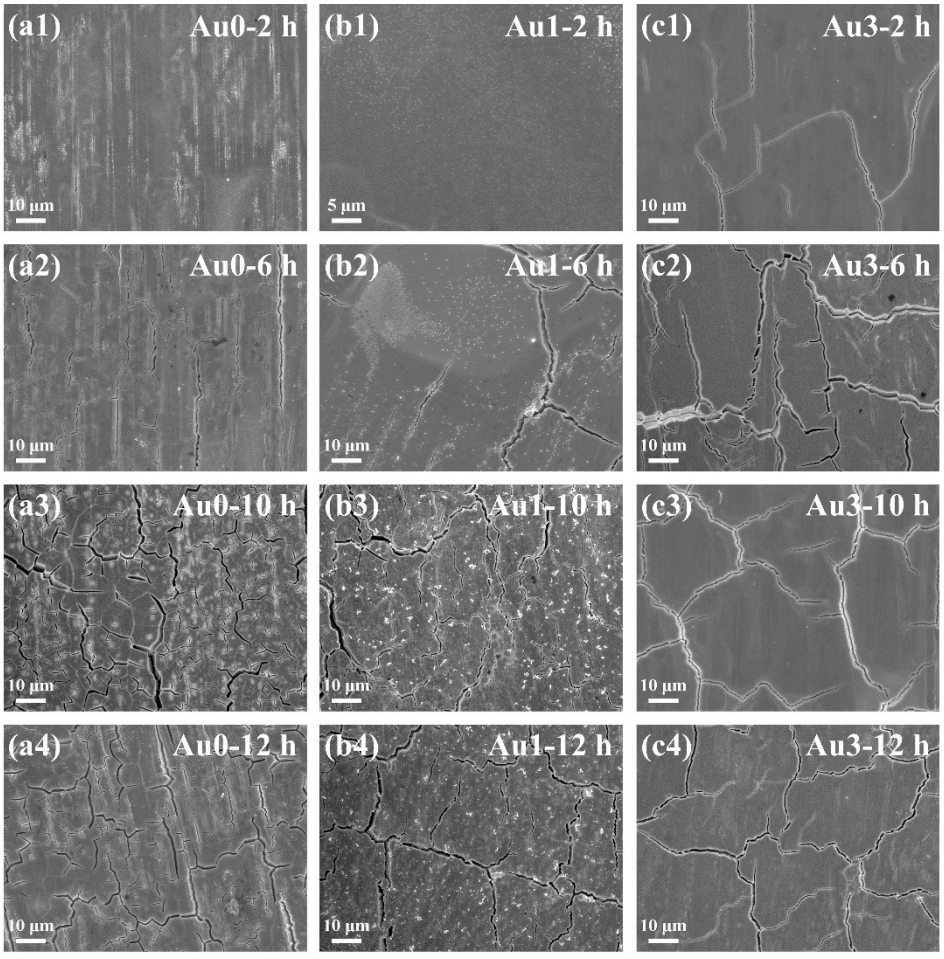

Figure S13 Plan-view SEM images of R-Au0 (a1-a4), R-Au1 (b1-b4) and R-Au3 (c1-c4)for different dealloying time.

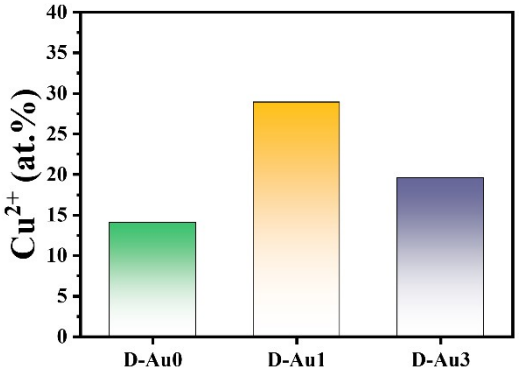

Figure S14 The content of Cu^{2+} (at.%) in as-dealloyed ribbons.

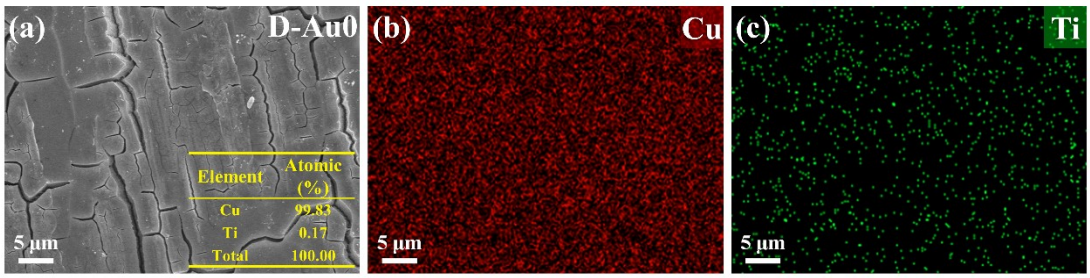

Figure S15 (a) Plain-view SEM image and EDX result of the plane, (b,c) corresponding elemental mapping images of D-Au0.

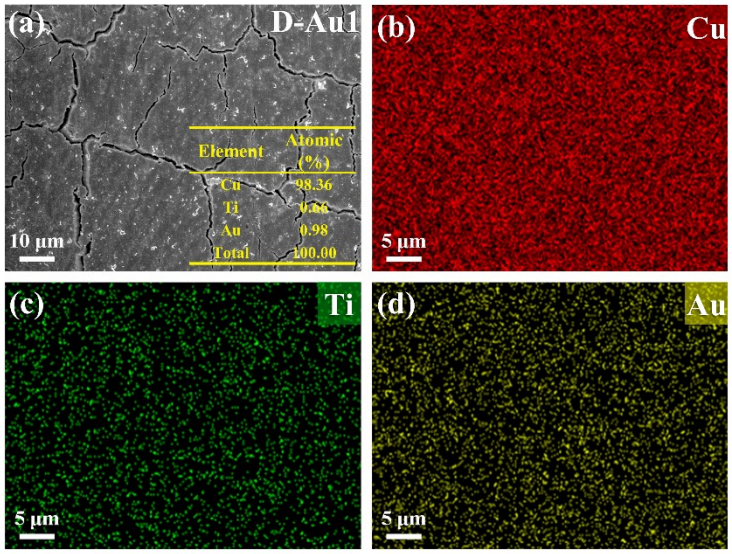

Figure S16 (a) Plain-view SEM image and EDX result of the plane, (b-d) corresponding elemental mapping images of D-Au1.

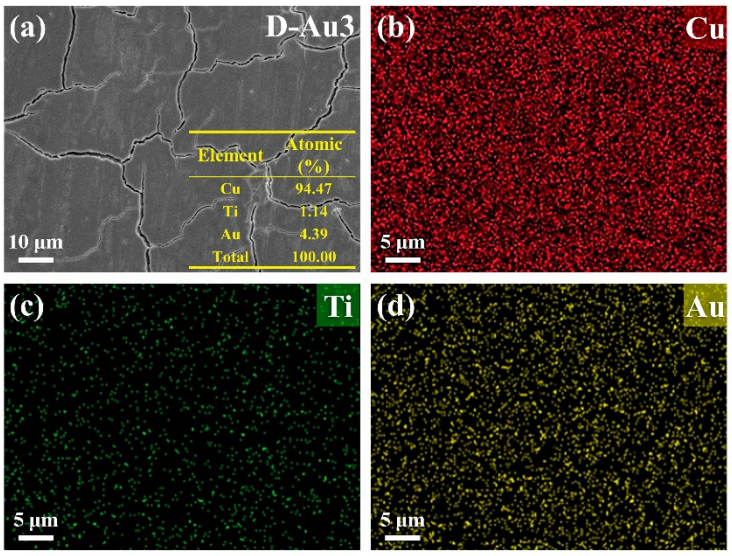

Figure S17 (a) Plain-view SEM image and EDX result of the plane, (b-d) corresponding elemental mapping images of D-Au3.

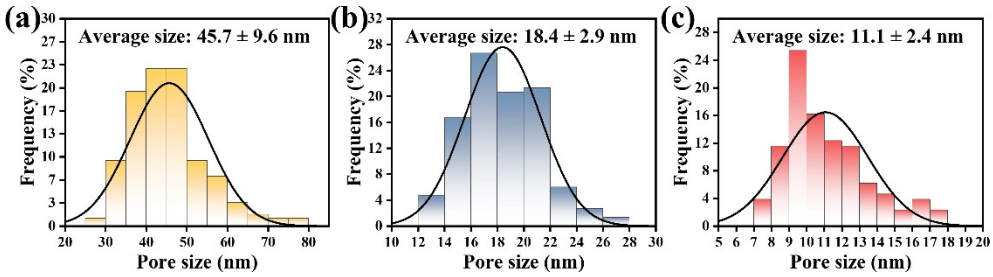

Figure S18 Pore size distribution of (a) D-Au0, (b) D-Au1, and (c) D-Au3 ribbon.

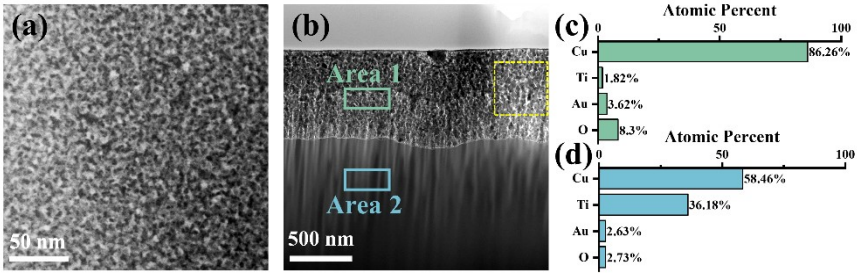

Figure S19 (a)TEM image of R-Au3 ribbon, (b) cross-sectional SEM image of D-Au3 ribbon, EDX result of area 1(c) and area 2(d) in (b).

The area enclosed by the yellow box in Figure S19b is enlarged in Fig 3f.

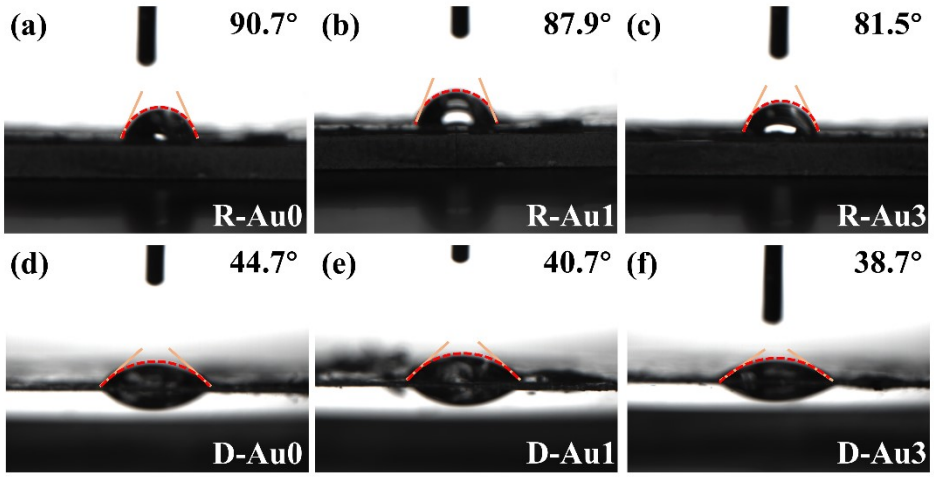

Figure S20 Droplet contact angles in 1 M KOH solution of (a) R-Au0, (b) R-Au1, (c) R-Au3, (d) D-Au0, (e) D-Au1, and (f) D-Au3.

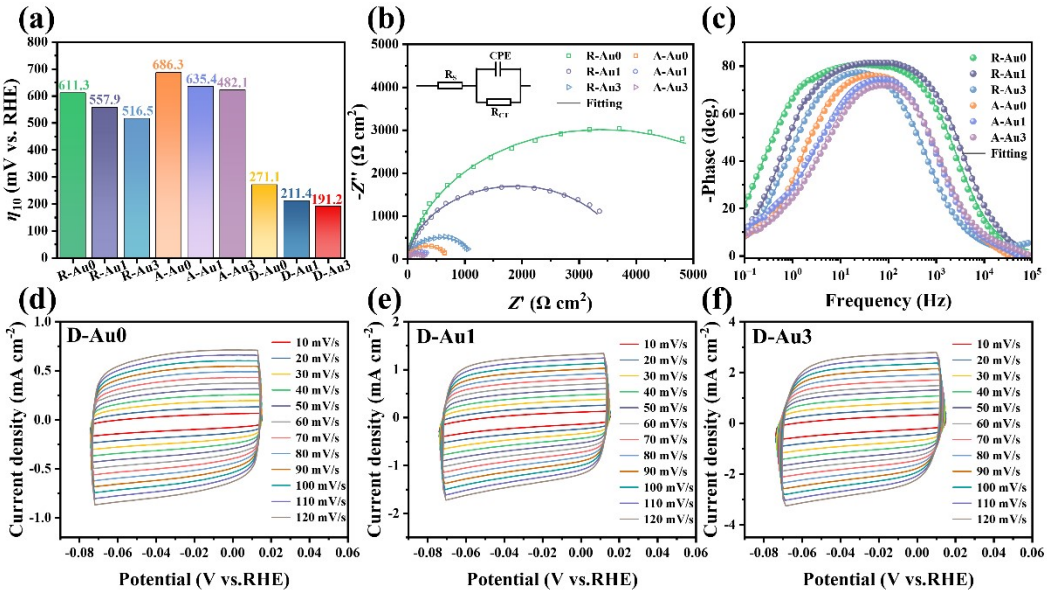

Figure S21 (a) Overpotential η_{10} of all the ribbons, (b) Nyquist plots and (c) Bode phase angle plots of as-spun and as-annealed ribbons, CV curves at different scan rate (10 mV·s^{-1}-120 mV·s^{-1}) for (d) D-Au0, (e) D-Au1, and (f) D-Au3 ribbon.

Turnover frequency (TOF) in this work was calculated based on the method of Liu et al.[1] and Tian et al.[2].In the HER region, the TOF per active sites can be calculated via the following equation:

$$\mathrm{TOF} = \frac{jA_{\mathrm{geo}}}{nxF}$$

$$= \frac{\#\text{total hydrogen turnovers per second}}{\#\text{active sites}}$$

$$= \frac{jA_{\mathrm{geo}}N_A/2F}{A_{\mathrm{ECSA}} \cdot \#\text{active sites}}$$

$$= j \times \frac{A_{\mathrm{geo}}}{A_{\mathrm{ECSA}}} \times \frac{1}{\#\text{surface sites}} \times \frac{N_A}{2F}$$

$$= j \times \frac{A_{\mathrm{geo}}}{A_{\mathrm{ECSA}}} \times \frac{1}{\#\text{surface sites}} \times 3.12 \times 10^{15}$$

where j is the geometric current density (mA/cm^2), A_{geo} is the geometric area of catalytic surface (cm^2), N_A is the Avogadro constant (N_A = 6.022 × 10^{23} mol^{-1}), F is the Faraday constant (F = 96485.3 C·mol^{-1}), A_{ECSA} is the electrochemically active surface area of catalyst (cm^2), #surface sites is the number of active sites per real surface area (atoms/cm^2).

Element parameters of Cu, Au as are listed below:

Element	**Crystal structure**	**Lattice constant**	**Numbers of atoms/Unit**	**Volume/Unit (nm^3)**	**#Surface sites (atoms/cm^2)**
Cu	FCC	0.3615	4	0.04724	1.93×10^{15}
Au	FCC	0.4068	4	0.06732	1.53×10^{15}

$$\#\text{surface sites}_{\mathrm{D-Au0}} = f_{\mathrm{Cu}}\#\text{surface sites}_{\mathrm{Cu}} = 1.928 \times 10^{15}$$

$$\#\text{surface sites}_{\mathrm{D-Au1}} = f_{\mathrm{Cu}}\#\text{surface sites}_{\mathrm{Cu}} + f_{\mathrm{Au}}\#\text{surface sites}_{\mathrm{Au}} = 1.921 \times 10^{15}$$

$$\#\text{surface sites}_{\mathrm{D-Au3}} = f_{\mathrm{Cu}}\#\text{surface sites}_{\mathrm{Cu}} + f_{\mathrm{Au}}\#\text{surface sites}_{\mathrm{Au}} = 1.908 \times 10^{15}$$

Finally, the TOF can be expressed as a function of current density as follows:

$$\mathrm{TOF}_{\mathrm{D-Au0}} = j \times \frac{0.4}{59.8} \times \frac{3.12 \times 10^{15}}{1.928 \times 10^{15}} = 0.01081j$$

$$\mathrm{TOF}_{\mathrm{D-Au1}} = j \times \frac{0.4}{124.8} \times \frac{3.12 \times 10^{15}}{1.921 \times 10^{15}} = 0.005208j$$

$$\mathrm{TOF}_{\mathrm{D-Au3}} = j \times \frac{0.4}{263.8} \times \frac{3.12 \times 10^{15}}{1.908 \times 10^{15}} = 0.002477j$$

The corresponding TOF curves are as shown in Fig. S22b.

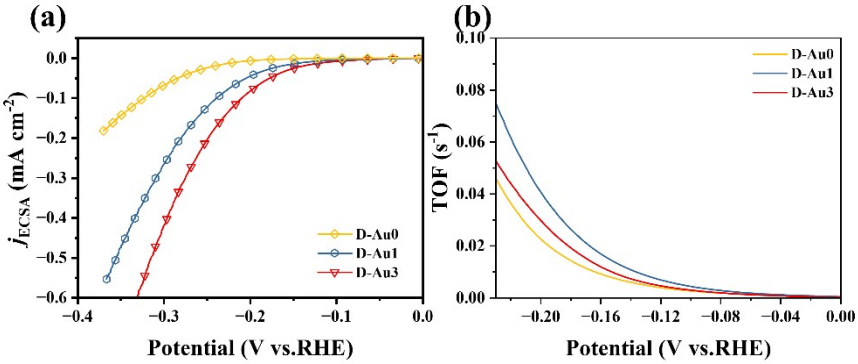

Figure S22 (a) ECSA-normalized LSV curves of D-Au0, D-Au1, and D-Au3, (b) the calculated TOF curves of as-dealloyed ribbons for HER.

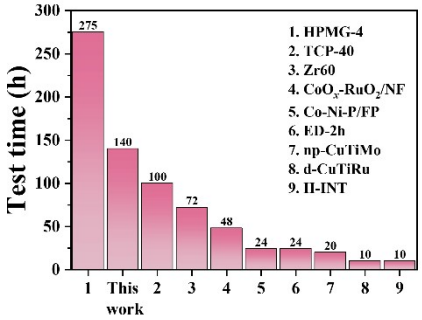

Figure S23 The comparison with other stability test durations.

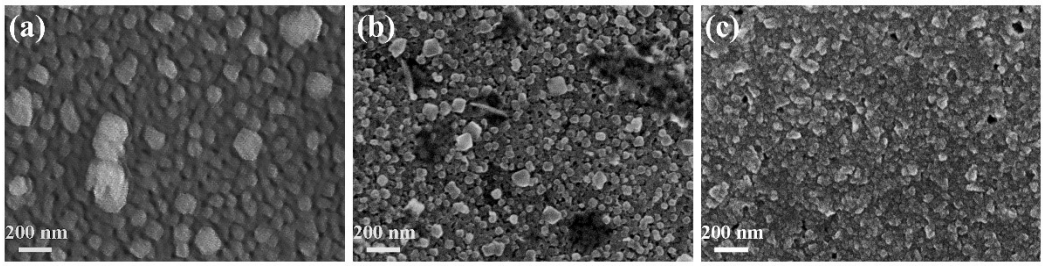

Figure S24 The SEM images of (a) D-Au0, (b) D-Au1, and (c) D-Au3 ribbon after HER stability test.

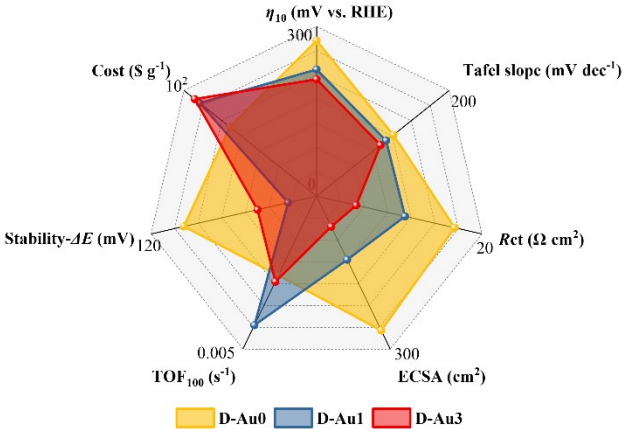

Figure S25 The comparison of the performances of the three catalysts (D-Au0, D-Au1, D-Au3).

Table S1 EDX results in Figure1i (SEM area and point scanning results).

Element	Cu (at.%)	Ti (at.%)	Au (at.%)	Total
Figure 1h	58.1	38.6	3.3	100
Point 1	57.0	39.7	3.3	100
Point 2	56.8	40.1	3.1	100
Point 3	66.8	30.3	2.9	100
Point 4	67.3	29.9	2.8	100

Table S2 Thermal parmeters deduced from the as-spun ribbons like crystallization temperature (T_x), melting starting temperature (T_m), liquidus temperature (T_l), solidification temperature (T_s), solidification temperature range ($\Delta T_{l\text{-}m} = T_l - T_m$), supercooling temperature ($\Delta T_{l\text{-}s} = T_l - T_s$)， and reduced glass transition temperature ($T_{rx} = T_{x1}/T_l$).

	T_{x1} (K)	T_{x2} (K)	T_m (K)	T_l (K)	T_s (K)	$\Delta T_{l\text{-}m}$ (K)	$\Delta T_{l\text{-}s}$ (K)	T_{rx}
R-Au0	684.8	694.1	1154.1	1220.5	1154.3	66.4	66.2	0.561
R-Au1	685.6	695.9	1160.6	1217.1	1156.1	56.5	61.0	0.563
R-Au3	690.1	702.8	1163.3	1218.7	1158.2	55.4	60.5	0.566

Table S3 The binding energy of Cu 2p, Ti 2p, Au 4f XPS spectra for as-spun and as-dealloyed ribbons.

Sample	Binding Energy (eV)			
	Cu 2p3/2	Cu^{2+} 2p3/2	Ti^{4+} 2p3/2	Au 4f7/2
R-Au0	932.7	934.6	458.6	-
D-Au0	932.6	935.0	458.7	-
R-Au1	932.9	934.4	458.8	85.2
D-Au1	932.5	934.8	457.9	84.6
R-Au3	932.7	934.1	459.0	84.9
D-Au3	932.5	934.9	458.1	84.6

Table S4 The pesk area of Cu 2p, Ti 2p, Au 4f XPS spectra for as-spun and as-dealloyed ribbons.

Sample	Peak Area (counts·eV)			
	Cu 2p3/2	Cu^{2+} 2p3/2	Ti^{4+} 2p3/2	Au 4f7/2
R-Au0	7.1×10^{3}	4.1×10^{3}	1.5×10^{4}	-
D-Au0	5.9×10^{4}	1.2×10^{4}	6.9×10^{3}	-
R-Au1	7.7×10^{3}	6.8×10^{3}	4.9×10^{3}	1.7×10^{2}
D-Au1	4.5×10^{4}	2.1×10^{4}	8.1×10^{2}	1.9×10^{3}
R-Au3	2.0×10^{3}	9.2×10^{2}	5.7×10^{3}	2.4×10^{2}
D-Au3	6.0×10^{4}	1.7×10^{4}	9.9×10^{2}	2.2×10^{3}

Table S5 The comparison with other stability test durations and whether the corresponding change values are reported.

Materials	Time (h)	Indicate the change amount	References
HPMG-4	275	No	3
D-CuAu	140	Yes	This work
TCP-40	100	No	4
Zr60	72	No	5
CoO_x-RuO_2/NF	48	No	6
Co-Ni-P/FP	24	No	7
ED-2h	24	No	8
np-CuTiMo	20	No	9
d-CuTiRu	10	No	2
H-INT	10	No	1

Table S6 The comparison of overpotential, conductance and costs of this work with other typical HER catalysts in 1 M KOH.

Materials	Overpotential η_{10} (mV)	Conductance (S·cm^{-2})	Costs (\$·g^{-1})	References
D-CuRu	35	0.7143	1.249	2
D-CuPt	63	0.0641	3.954	4
$Rh_{26.1}Ru_{28.7}Pt_{8.6}Pd_{16.3}Ir_{20.3}$	65	0.0236	104.082	10
$Ir_{25}Ni_{33}Ta_{42}$	232	0.0175	52.283	1
$Cu_{20}W_{80}$	181	0.0097	0.022	11
NiB@Cu	221.2	0.0082	0.009	12
NP-NiP	320	0.0042	0.013	13
$Fe_{40}Ni_{20}Co_{20}P_{15}C_5$	355	0.0010	0.010	14
$(FeCoNi)_{70}Cu_{30}$	94	0.0004	0.014	15
D-Au3	191.2	0.0917	10.425	This work

References

1. D. Q. Liu, Z. Q. Song, S. R. Cheng, Y. L. Wang, A. Saad, S. T. Deng, J. Shen, X. Huang, X. K. Cai and P. Tsiakaras, *Chem. Eng. J.*, 2022, **431**, 134210.
2. J. S. Tian, Y. C. Hu, W. F. Lu, J. H. Zhu, X. D. Liu, J. Shen, G. Wang and J. Schroers, *Carbon Energy*, 2023, **5**, e322.
3. X. R. Zhao, J. S. Liu, H. T. Zhang, J. H. Jiang, J. Q. Lin, J. N. Fu, Y. Zhang, X. Li, W. Q. Ruan and J. Ma, *Chem. Eng. J.*, 2025, **515**, 163667.
4. H. Zhang, J. H. Qin, J. S. Tian and J. Shen, *Int. J. Hydrogen Energy*, 2024, **82**, 952-958.
5. C. Wang, P. Zou, W. Xu, Y. Zhang, J. T. Huo, J. Q. Wang, Y. Liu and C. L. Qin, *J. Alloys Compd.*, 2024, **995**, 174790.
6. T. Q. Yu, Q. L. Xu, G. F. Qian, J. L. Chen, H. Zhang, L. Luo and S. B. Yin, *ACS Sustain. Chem. Eng.*, 2020, **8**, 17520-17526.
7. Y. Zhang, Z. Zhang, X. T. Zhang, X. L. Gao, Z. H. Shang, X. Z. Huang, E. Y. Guo, C. H. Si, M. Z. Wei, Q. F. Lu and X. J. Han, *J. Alloys Compd.*, 2024, **972**, 172854.
8. S. S. Jiang, L. Zhu, Z. Z. Yang and Y. G. Wang, *Int. J. Hydrogen Energy*, 2021, **46**, 36731-36741.
9. K. S. Aneeshkumar, J. Tian and J. Shen, *J. Alloys Compd.*, 2021, **886**, 161270.
10. Y. Zou, L. Jing, J. Zhang, S. Luo, L. Wang, Y. Li, R. Goei, K. W. Tan and A. I. Yoong Tok, *J. Mater. Chem. A*, 2024, **12**, 5668-5678.
11. X. Jian, W. Zhang, Y. Yang, Z. Li, H. Pan, Q. Gao and H. J. Lin, *ACS Catal.*, 2024, **14**, 2816-2827.
12. H. Xun, T. Liu, J. Zhang, C. Yan, Y. Ju, L. Shi, Q. Che, D. Zhao and M. Zuo, *Mater. Sci. Eng. B - Adv.*, 2025, **318**, 118294.
13. Y. Pang, S. Zhu, Z. Cui, Y. Liang, Z. Li and S. Wu, *Prog. Nat. Sci.:Mater. Int.*, 2021, **31**, 201-206.
14. K. S. Aneeshkumar, J.-c. Tseng, X. Liu, J. Tian, D. Diao and J. Shen, *RSC Adv.*, 2021, **11**, 7369-7380.
15. Z. Ding, Z. Chen, X. Liu, J. Liu, T. Wang, A. Chen, B. Gan and Y. Zhang, *Chem. Eng. J.*, 2025, **506**, 160016.